Naval Research Laboratory
Washington, DC 20375-5320

NRL/5310/MR—2024/2

Numerical Integration of the Eikonal Equation with Stochastic Refractive Index

MAXWELL B. BLOCK

DAVID R. BERGMAN

Radar Analysis Branch
Radar Division

March 14, 2024

REPORT DOCUMENTATION PAGE

PLEASE DO NOT RETURN YOUR FORM TO THE ABOVE ORGANIZATION

1. REPORT DATE	2. REPORT TYPE	3. DATES COVERED	
		START DATE	END DATE
14-03-2024	NRL Memorandum Report	06-05-2023	01-31-2024

4. TITLE AND SUBTITLE

Numerical Integration of the Eikonal Equation with Stochastic Refractive Index

5a. CONTRACT NUMBER	5b. GRANT NUMBER	5c. PROGRAM ELEMENT NUMBER
5d. PROJECT NUMBER	**5e. TASK NUMBER**	**5f. WORK UNIT NUMBER**
		1AA1

6. AUTHOR(S)

Maxwell B. Block and David R. Bergman

7. PERFORMING ORGANIZATION / AFFILIATION NAME(S) AND ADDRESS(ES)

Naval Research Laboratory
4555 Overlook Ave SW
Washington, DC 20375-5320

8. PERFORMING ORGANIZATION REPORT NUMBER

NRL/5310/MR—2024/2

9. SPONSORING / MONITORING AGENCY NAME(S) AND ADDRESS(ES)	10. SPONSOR / MONITOR'S ACRONYM(S) NUMBER	11. SPONSOR / MONITOR'S REPORT NUMBER(S)
Office of Naval Research 875 N Randolph Street Arlington, VA 22217-1995	ONR	

12. DISTRIBUTION / AVAILABILITY STATEMENT

DISTRIBUTION STATEMENT A: Approved for public release; distribution is unlimited.

13. SUPPLEMENTAL NOTES

14. ABSTRACT

A method for numerically solving the Eikonal equations is developed and applied to wave propagation in a random media. The results are compared to standard ray theory and differences discussed.

15. SUBJECT TERMS

Electrodynamics, Stochastic Differential Equations, Random Media, Eikonal Equation, Ray Theory

16. SECURITY CLASSIFICATION OF:			17. LIMITATION OF ABSTRACT	18. NUMBER OF PAGES
a. REPORT	b. ABSTRACT	c. THIS PAGE		
U	U	U	SAR	30

19a. NAME OF RESPONSIBLE PERSON	19b. PHONE NUMBER *(Include area code)*
David R. Bergman	(202) 934-4820

This page intentionally left blank.

CONTENTS

FIGURES

NUMERICAL INTEGRATION OF THE EIKONAL EQUATION WITH STOCHASTIC REFRACTIVE INDEX

1. INTRODUCTION

This report outlines the development of numerical methods for solving the Eikonal equation. The Eikonal equation is a non-linear partial differential equation (PDE) describing the evolution of wavefronts related to wave theory and the general theory of hyperbolic PDEs [1]. This work is part of a larger effort to research, understand, and develop stochastic ray equation solvers suitable for application to radio frequency (RF) propagation and scattering. More generally, the development of stochastic Maxwell's equations solvers [2]. The classical ray paths can be thought of as flow lines of the wavefront gradient, these two mathematical objects being deterministically connected, see Figure 1.

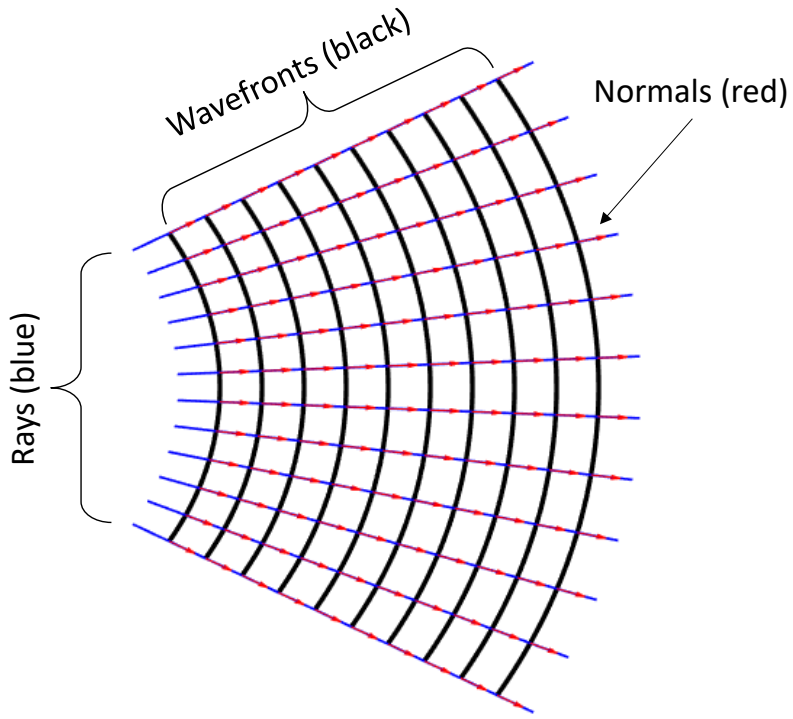

Figure 1 – Relationship between wavefronts (black), ray paths (blue), and the normal vectors (red) to the surface.

Conceptually, one might expect that adding stochastic noise to the ray equation would produce Brownian paths due to the noise introducing random kicks to the ray momentum akin to a random walk. One driver of this work is to investigate to what extent the classical descriptions of the wavefront and the ray path remain connected when stochastic effects are introduced, as well as to determine the most reliable numerical approach to developing prediction codes for stochastic propagation. The types of questions that come to mind include:

(1) Can stochastic rays be used to build a stochastic wavefront?

Manuscript approved March 12, 2024.

(2) Can a stochastic Eikonal be differentiated in some sense to generate stochastic ray paths?
(3) Are the two procedures mentioned in (1) and (2) compatible and commutative to all orders?
(4) Does the conjugate point theorem generalize to the stochastic system, allowing one to predict the onset of caustics?

This last question will be discussed in more detail at the end of section 2 and constitutes one of the major drivers of this research.

The first step is understanding how to numerically solve the Eikonal and develop and stable convergent solver, the primary results presented in this report. The remainder of the report is organized as follows. Chapter 2 presents a derivation of the Eikonal from several different approaches and discussed how they relate to each other. Chapter 3 contains an overview of several methods for numerically solving the Eikonal equation. Chapter 4 presents benchmarking results for the classical Eikonal and ray theory with toy model refractive profiles that have known exact solutions. Chapter 5 discusses the introduction of stochasticity into the environment through the refractive index. Chapter 6 contains a discussion and summary. An appendix is included that contains a derivation supporting some of the results in chapter 5.

2. THE EIKONAL

In this section the Eikonal equation, the classical ray equation, and their derivation are discussed. Readers may be familiar with both of these concepts from optics, RF propagation, or acoustics. Despite its ubiquitous nature in every field of study where wave propagation is encountered there seems to be some misunderstanding (or dogma) regarding what these equations represent. For brevity, lengthy derivations will not be presented and the reader is referred to the literature for details. The purpose of this section is to provide an overview of the multiple ways the Eikonal and ray theory appear and how these different representations are similar and, more importantly, where they differ from one another. The presentation will be in the form of a discussion with enough depth to support following sections and the main motivation of the research. Also discussed in this section are, how rays are used to develop estimates of a full field solution in some cases, and the relationship between ray theory and differential geometry.

2.1 Classical Derivation

The most common approach to deriving the Eikonal and ray equations is through the high frequency approximation of the scalar Helmholtz equation, Eq. (1).

$$\nabla^2\psi + k^2 n^2 \psi = 0 \tag{1}$$

The reader is referred to chapter 2 of Kravtzav and Orlav [3], and page 21-22 of Foreman [4] for details on this derivation. This presentation mixes notation from both references, which are otherwise very similar. The following quantities are defined, the wavenumber, $k = \omega/c_0$, and the refractive index, $n = c_0/c$. The Helmholtz equation is derived from the second order wave equation by assuming a time harmonic source with angular frequency ω. The refractive index can be a function of position through its local dependence on the wave speed, $c(\vec{x})$. The reference speed, c_0, is constant and usually taken to be the speed of light in vacuum. A solution of the form presented in Eq. (2) is assumed.

$$\psi = e^{ik\varphi} \sum_{m=0}^{\infty} \frac{A_m}{(ik)^m} \tag{2}$$

Applying Eq. (2) to Eq. (1) and setting each factor of each unique power of k to zero leads to a hierarchy of equations.

$$\begin{aligned} \vec{\nabla}\varphi \cdot \vec{\nabla}\varphi &= n^2 \\ 2\vec{\nabla}A_0 \cdot \vec{\nabla}\varphi + A_0\nabla^2\varphi &= 0 \\ 2\vec{\nabla}A_1 \cdot \vec{\nabla}\varphi + A_1\nabla^2\varphi &= -\nabla^2 A_0 \\ &\vdots \\ 2\vec{\nabla}A_m \cdot \vec{\nabla}\varphi + A_m\nabla^2\varphi &= -\nabla^2 A_{m-1} \end{aligned} \tag{3}$$

The lowest order term is the classic Eikonal equation. The next order can be converted into a total vanishing divergence, $\vec{\nabla} \cdot \left(A_0^2 \vec{\nabla}\varphi\right) = 0$. It is customary to define trajectories in space that are flow lines of the Eikonal gradient, $\vec{\nabla}\varphi \equiv d\vec{r}/ds$, known as ray paths. The parameter s is arc-length along the ray. Ray are often parameterized using other independent variables such as time or some other monotonically increasing quantity. Varying this first order non-linear and using the original equation as a constraint leads to a second or ordinary differential equation (ODE) for these paths, the classic ray equation, the form of the ray equations presented here echo that found in Kravtzav and Orlav [3].

$$\begin{aligned} \frac{d\vec{r}}{d\tau} &= \vec{p} \\ \frac{d\vec{p}}{d\tau} &= \frac{1}{2}\vec{\nabla}n^2 \end{aligned} \tag{4}$$

The parameter τ is related to arc-length, s, by $nd\tau = ds$. A single non-linear first order PDE for the phase surfaces in all of space has been replaced with a second order quasi-linear ODE that must be solved multiple times (really an infinite number of times) to describe points on the Eikonal surface. The next order term in the expansion, with the help of the Eikonal, can be massaged into the form of a conservation law. Integrating this leads to the law of geometric spread of a cross sectional area of a ray bundle, and that the first order amplitude is nothing more than the inverse root of this geometric spread factor. Formally, the geometric spread is the determinant of the Jacobian obtained by differential the ray path coordinates with respect to initial conditions. Denoting the geometric spread factor by D a first order estimate for the field at some point down range from a point source along a specific ray path is $\psi \sim \exp ik\varphi/\sqrt{D}$.

With these ingredients one can develop a procedure for estimating the total field anywhere in space, including boundaries, by the method of ray tracing. In the frequency domain, one gathers all rays that connect a source point to a field point (or receiver), referred to as eigen-rays. The travel time, t, along each eigen ray is evaluated to produce the phase, $\theta = k\varphi \equiv \omega t$, and the geometric spread is calculated to provide the first order amplitude factor, a. This can be numerically intensive as it requires tracing many rays and numerical differentiation or solving an augmented set of equations that include a transport equation for the spreading factor. A complete description of each contribution requires tracking discrete phase shifts due to (1) boundary interactions, and (2) formation of caustics along the ray path. With all this accounting complete the total field at the field point is $\sum_{n=1}^{N} a_n \exp i\theta_n$, where the index sums over all eigen-rays. This approach has been successful in optics, acoustics, seismology, and all fields of research where high frequency wave propagation is considered as long as the field point is not too close to a caustic.

In free space, rays from a point source will diverge from each other with a geometric spread factor of $\sim R^2$ in all directions, leading to a field value, away from the source, of $\sim \exp ikR/R$, with $\tau = R/c$. In this trivial example the first two terms in the expansion reproduce the correct field at all points in space and for all frequencies, the solution being identical to the frequency domain Green's function. When position dependent refraction and/or boundaries are present an eigen-ray analysis to first order will not generally produce a complete field at the field point, but rather an approximation. These environmental factors can

cause enhanced focusing (or defocusing) of the wavefront away from the source, as if a lens was present. When focusing occurs, the first order ray approximation can break down at special points causing an infinite amplitude (zero geometric spread) in the vicinity of the focal region. This unphysical behavior is called a caustic. The focusing effect is physical but the infinite amplitude predicted by first order ray theory is not physical. There are well known methods to correct for this behavior by including higher order terms from the expansion. An early approach by Ludwig expands the wave equation near the caustic, providing correction terms that lead to a finite amplitude in all regions of space [5]. More recent advances include Gaussian beam tracing where the initial equations include more complexity and track various amplitude factors along the ray path [6]. A take away from this discussion on the ray theory approach is that despite its apparent simplicity and intuitive appeal, constructing full field solutions from ray traces can be very tricky, involving a lot of accounting and a slew of correction factors each requiring more numerical work.

However, despite these criticisms, there is something consistent in the theory. Namely the Eikonal. The zeroth order term in the expansion incurs no corrections as a function of frequency, indicating that whatever information is contained in it is valid at all frequencies. This information is related to the travel time of an impulsive source from source to receiver along each eigen-ray.

This section closes with a comment on "covariant" forms of the Eikonal. The starting point in this section was the Helmholtz equation in the frequency-domain, suitable for time-harmonic sources. Rather than start with Helmholtz, the full scalar wave equation is used as the starting point.

$$\nabla^2\psi - \frac{1}{c^2}\frac{\partial^2\psi}{\partial t^2} = 0 \tag{5}$$

Equation (5) is the standard form of the wave equation, but for both optics and acoustics it is a derived equation and not fundamental. Rather than work with this form a covariant version, Eq. (6), is employed. In some cases it is possible to reorganize terms on the fundamental field equations to create a covariant form of the wave equation [7].

$$D^\mu D_\mu\psi = \frac{1}{\sqrt{-g}}\partial_\mu\sqrt{-g}\,g^{\mu\nu}\partial_\nu\psi = 0 \tag{6}$$

The factor of $g^{\mu\nu}$ in Eq. (6) is the contravariant metric tensor, and g its determinant. The metric can arise from (1) expressing the second order derivative operator in terms of general curvilinear coordinates [8], (2) actual curvature of space-time (as occurs in relativistic astrophysics) [9], or (3) the emergence of an effective metric described by coordinate dependent environmental factors (*e.g.* refractive index) [10]. The covariant form takes some getting used to but, in the end, is easier to manipulate mathematically. It arises naturally from the study of light propagating in a curved space-time where gravity (space-time curvature) creates lensing effects, bending light rays and creating other aberrations. It also arises in the study of acoustics in a moving fluid, where analog models of black holes are predicted in super fluid Helium providing a possible laboratory testbed for investigating Hawking radiation [11, 12]. For the study of electromagnetic propagation it is natural to appeal to the tensor form of Maxwell's equations in a source free region, which are manifestly covariant.

$$D_\mu F^{\mu\nu} = 0 \tag{7}$$

To facilitate the derivation, Eq. (6) will be employed but it is noted that the same results emerge from Eq. (7), see reference [9]. The basic steps are the same, with the exception that the fields in Eq. (2) are functions of position and time, resulting in the following covariant version of Eq. (3).

$$\begin{gathered} g^{\mu\nu}\,\partial_\mu\varphi\,\partial_\nu\varphi = 0 \\ D^\mu\left(A_0^2\,\partial_\mu\varphi\right) = 0 \\ 2g^{\mu\nu}\,\partial_\mu A_1\,\partial_\nu\varphi + A_1 D^2\varphi = -D^2 A_0 \\ \vdots \\ 2g^{\mu\nu}\,\partial_\mu A_m\,\partial_\nu\varphi + A_m D^2\varphi = -D^2 A_{m-1} \end{gathered} \tag{8}$$

Clearly, using Eq. (7) will produce a different set of equations in terms of second rank field tensors, but the first two equations are common to all approaches (see Chapter 3 of [13]). Namely that the Eikonal equation represents the wavefronts and the first order amplitude is related to the geometric spread of the ray paths. Defining a Hamiltonian from the Eikonal equation and varying this, with $g^{\mu\nu}\,\partial_\mu\varphi \equiv dx^\nu/d\lambda$, produces a version of the ray equation that is identical to the geodesic equation in 4D space-time defined by the metric, $g^{\mu\nu}$ and its inverse $g_{\mu\nu}$. In terms of the ray paths, the Eikonal equation is a constraint that requires the ray path momentum to have zero magnitude in 4D, known as the null constraint. In the covariant form, rays are space-time paths of zero length, called null-geodesics [1, 10-12]. A comment about the metric introduced in Eq. (6) and the refractive index is appropriate here. In the covariant form of these equations the material properties are contained in the effective metric, *i.e.* the local wave speed $c(x^\mu)$ is contained in $g_{\mu\nu}$. An example of an effective metric, Eq. (9), and the geodesic equation, Eq. (10), are provided below.

$$g_{\mu\nu} = \begin{bmatrix} -1 & \mathbf{0}^T \\ \mathbf{0} & c^2\mathbf{I_3} \end{bmatrix} \tag{9}$$

$$\frac{d^2x^\mu}{d\lambda^2} + \Gamma^\mu_{\alpha\beta}\frac{dx^\alpha}{d\lambda}\frac{dx^\beta}{d\lambda} = 0 \tag{10}$$

In Eq. (10) the factors $\Gamma^\mu_{\alpha\beta}$ are the Christoffel symbols of the second kind, derived from the effective metric in Eq. (9) and λ is referred to as an affine parameter along the geodesic path (not to be confused with wavelength) [7]. In Eq. (9) $\mathbf{I_3}$ is the 3 by 3 identity matrix and $\mathbf{0}$ a column vector of zeros.

2.2 Method of Characteristics

Another approach to deriving the Eikonal is by applying the method of characteristics to Maxwell's equations. The details a beyond the scope of this report and the reader is referred to the literature, especially Courant and Hilbert Volume II [1]. Briefly, this method can be applied to any quasi-linear system of PDEs describing general conditions for a solution to exist away from a hyper-surface of initial data, called a Cauchy surface. The method does not assume, or require, a series expansion in frequency or any other parameter, rather using general coordinate transformations to cast the systems of PDEs in coordinates near the Cauchy surface. The method applies to PDEs in the time domain so no transform or assumption about sources being mono-chromatic are necessary. Maxwell's equations are hyperbolic in nature and the method gives rise to the familiar light cone structure encountered in relativity. The characteristic surfaces are surfaces on which future values are evaluated after taking a small step away from the initial surface, a process that can be repeated to develop a full solution in space-time except near points where the surface is ill-defined. These surfaces are referred to as 'Characteristic surfaces' and the flow lines along which the initial surface is propagated called bicharacteristics. The characteristic surfaces and bicharacteristic curves are in one-to-one correspondence with the wavefronts and rays described in the previous section. When the environmental parameters are functions of spatial coordinates and time the bicharacteristics are geodesics of a pseudo-Riemannian manifold where the metric tensor components are functions of the same parameters, *e.g.* permittivity and permeability or refractive index. Bicharacteristics are curves along which

jump discontinuities in the fields will propagate. In contrast, the frequency-domain description of previous section is more suitable for describing continuous waves. An example of the equation for the characteristic and bicharacteristic are presented below.

$$\vec{\nabla}\varphi \cdot \vec{\nabla}\varphi - \frac{1}{c^2}\left(\frac{\partial \varphi}{\partial t}\right)^2 = 0 \tag{11}$$

The method of characteristics typically leads to multiple characteristic conditions, in many cases the same condition repeated multiple times. A partial Hamiltonian is defined by each characteristic factor and momentum variables defined by $\vec{p} \equiv \vec{\nabla}\varphi$ and $p_0 \equiv \partial\varphi/\partial t$, where the time component, p_0, may be thought of as generalized energy. Variation of the above equation leads to an equation for the bicharacteristics as null-geodesics of a Lorentzian manifold where the local wave speed $c(\vec{x}, t)$ creates an effective metric tensor, Eq. (10) of section 2.1. Although the field is not directly expressed in terms of the hyper-surface φ is it generally identified with the wavefront and the bicharacteristics with rays. Like the covariant Eikonal approximation used by Visser [12] and Perlick [13], this approach maintains the intrinsic general covariance of the classical ray paths. In fact, rays follow the same curves as photons, massless particles, in relativity, namely null geodesics.

2.3 Exact Eikonal

Section 2.1 presented the classic frequency-domain derivation of the high frequency expansion of the Helmholtz equation and the ray equations derived from them while section 2.2 presented the results of applying the method of characteristics to Maxwell's equations. This section offers yet another point of view related to ray theory called the "exact" Eikonal by Terry Foreman [14]. The original work by T. Foreman was published in acoustics but is applicable to optics and other wave phenomenon. The field is described by an amplitude and a phase, $\psi = Ae^{i\Phi}$, and a set of coupled equations derived from the Helmholtz equation, Eq. (1).

$$\begin{aligned} \vec{\nabla}\Phi \cdot \vec{\nabla}\Phi &= k^2 n^2 + \frac{\nabla^2 A}{A} \\ 2\frac{\vec{\nabla}A}{A} \cdot \vec{\nabla}\Phi + \nabla^2\Phi &= 0 \end{aligned} \tag{12}$$

The key feature of this approach is that there is no approximation and all components of the field are present in the description. The second equation can be written as a total divergence, $\vec{\nabla} \cdot \left(A^2 \vec{\nabla}\Phi\right) = 0$. One take way from the original work is that "exact rays" have a conserved quantities to all orders, in contrast to classical ray theory which does contain a conserved quantity to first order. Another very useful feature of the exact rays is that they do not cross and do not develop caustics, an artifact of classical ray theory and the method of characteristics, and exist in classical shadow zones [14].

A similar approach in optics that includes the polarization of the electromagnetic field was recently published by Nichols *et al* [15, 16]. The electric field is described by a second order wave equation with the following description, where ρ, φ, and γ are functions of position, following their notation.

$$\vec{E} = \rho^{1/2} e^{i(k_0 z + \varphi)} \begin{bmatrix} \cos\gamma \\ \sin\gamma \\ 0 \end{bmatrix} \tag{13}$$

The form of the field is designed to describe propagation along the *z*-axis, with *x* and *y* defined as transverse coordinates. The corresponding Eikonal for this field is presented below in slightly different form, with $2\eta = n^2 - 1$ and $\vec{\nabla}_{\vec{X}}$ a transverse gradient operator.

$$\vec{\nabla}_{\vec{X}}\varphi \cdot \vec{\nabla}_{\vec{X}}\varphi + 2k_0 \frac{\partial \varphi}{\partial z} + \vec{\nabla}_{\vec{X}}\gamma \cdot \vec{\nabla}_{\vec{X}}\gamma - \frac{\vec{\nabla}^2_{\vec{X}}\rho^{1/2}}{\rho^{1/2}} - 2k_0^2\eta = 0 \tag{14}$$

The complete set of equations was solved in [16] for an ideal test case demonstrating ray path bending in free space due to a specific initial polarization state.

Lastly, a covariant version of Eq. (12) is presented. To the authors' knowledge this has not been presented in the literature. The derivation is quite simple, staring with Eq. (6) and using the same form for ψ with amplitude and phase each a function of space-time coordinates.

$$\begin{gathered} g^{\mu\nu}\partial_\mu\Phi\,\partial_\nu\Phi - \frac{D^2A}{A} = 0 \\ D^\mu\left(A^2\,\partial_\mu\Phi\right) = 0 \end{gathered} \tag{15}$$

The first equation is a 4D covariant "exact" Eikonal and the second represents a covariant conserved 4-current.

2.4 Summary of Ray Theory and the Eikonal

This section summarizes the previous sections, pointing out similarities and differences between all approaches that claim to lead to the Eikonal and what they represent. The geometric significance of the covariant form is discussed along with unique symmetries present in the covariant form that are not present at all or not obvious in other forms of the Eikonal. Finally, the rational and justification for the selection presented in this research is given.

The reader may be naturally perplexed at the variety of Eikonals presented in this section. This summary should help shed light on the nature of each. The method of characteristics is a general method for solving systems of PDEs on any background space, or space-time. Regardless of whether one develops an "exact Eikonal" to describe the field or chooses to work with an asymptotic expansion, the resulting full solutions must evolve from one characteristic surface to another along bicharacteristics. The individual pieces of the solution do not, but the total solution must. If one inspects the high frequency expansion of the wave equation, classical Eikonal, the following should be realized. Even though there are an infinite number of terms required to build up the field as a series, the Eikonal incurs no corrections. It contains information that is truly universal to all orders.

A feature of the covariant classical Eikonal (or characteristic and bicharacteristic) is that it exhibits several properties that the original field equations may not. The first, is general covariance. In section 2.1 the time-domain wave equation and a covariant version of the same (equations (5) and (6) respectively) were introduced. The wave equation in Eq. (5) is not invariant under general coordinate transforms, however Eq, (6) is manifestly invariant. Regardless, the Eikonal and ray equation derived from either equation obey general covariance. This same feature is seen in acoustics in a moving fluid where the original equations do not respect Lorentz symmetry, or general covariance, but the resulting wavefronts and rays do when expressed in the time-domain. The common feature of the second order wave equation, Maxwell's field equations, and the equations of fluid dynamics is that they are all examples of hyperbolic PDE systems. The method of characteristics, section 2.2, provides the most general approach to arriving at this common result.

The high frequency approximations do contain a conserved quantity along the classical ray path but higher order amplitude terms are not individually conserved, whereas the Exact Eikonals, Eqs. (12) and (15), have a property that is fully conserved along the "exact" ray path. These new, "exact", paths are not, in general, the same as the classical rays. Which path is "correct"? Both. This apparent paradox is eloquently addressed in Foreman's work for the scalar acoustic field [14]. Briefly, the disparity arises from the fact that classical rays are best suited for describing short pulses, *i.e.* propagation of impulses, and the exact ray path is better suited for continuous waves. A significant difference between these approaches is that the classical ray paths will provide a travel time for the leading edge of pulse along all paths that connect the source to a receiver. These will correspond to observed delay times seen in a data collection system when environmental effects cause arrival of more than one copy of the pulse due to ray path bending and boundary interactions. This type of information is not contained in the exact ray path. In contrast, it is well known that classical ray theory breaks down at caustics and offers no amplitude estimate in shadow zones (without higher order corrections), whereas exact rays penetrate shadow zones providing a means to predict evanescent field strength. Another significant difference appears in the geometric interpretation of rays as null-geodesics. Both the high frequency expansion and the method of characteristics lead to the same Eikonal and ray path structure, which is well understood to be described by Lorentzian differential geometry with an effective metric tensor [1]. The exact Eikonals presented here do not share this interpretation. The first ray equation presented in Eq. (4) does not appear to be a null-geodesic equation and trying to demonstrate this is difficult. However, starting from the geodesic equation it is rather easy to arrive at Eq. (4) by a series of parameter changes and conformal transforms [17]. The difficulty in recognizing Eq. (4) as a null geodesic has led to a failure to see the benefits of new properties, including symmetries, in optics and acoustics and benefit from these. These are discussed in the remaining paragraphs.

For this research the classical ray and Eikonal are selected. This is due to their being described as geodesics and the benefits that accompany this description and for the connection to predicting travel time. First note that the Eikonal structure will exhibit general covariance regardless of whether or not the original field equation has general covariance. This is a general feature of all hyperbolic PDEs. Based on this it is clear that the classical Eikonal is missing some information about the field but what information it does contain obeys general covariance as well as several other features now described. As an example, the equations for an inviscid, isentropic, Newtonian fluid are not generally covariant with respect to space-time coordinate transforms or Lorentz transformations, but they do comprise a hyperbolic PDE system and the characteristic surfaces and bicharacteristics form null structures in space-time [1, 10]. Adding the constraint that the fluid be irrotational leads to a truly covariant wave equation like that in Eq. (6) [11, 12]. A consequence of being a null-hypersurface or a null-geodesic is that the geometry of these objects is completely immune to a conformal transformation, a transformation in which the metric is multiplied by an arbitrary positive definite scalar field. Conformal symmetry is a form of gauge symmetry arising from a continuous group of transformation and can be used to create a continuum of equivalent equations for the same set of rays [17]. In addition to conformal symmetry, the geometric form of the classical ray equation can be analyzed using Killing's theorem to identify isometries [18]. An isometry is a "rigid" symmetry of the geometry and directly related to a conserved quantity along the ray paths, *e.g.* momentum or energy. The frequency domain ray equation, Eq. (4), can be elevated to a null geodesic path in 4D with some mathematical gymnastics but this does not appear to be its natural home and the presence of conformal symmetry and isometry are not manifestly apparent. Once the covariant geometric form is identified the geometric spread is determined by geodesic deviation [10]. Through this set of equations, the focusing and/or defocusing of a ray bundle is measured by the Riemann curvature tensor induced by the local refractive index. Including the geodesic deviation equation with the ray equation produces a full set of "dynamic" ray equations that solve the amplitude factor as a transport equation along the ray path, in contrast to traditional methods that numerically differentiate ray bundles. Related to this, the Riemann curvature tensor provides a means to predict with some certainty when and where caustics will form along ray paths by the conjugate point theorem [19, 20]. The value to using the covariant form for all hyperbolic

PDEs lie in the fact that all of these features; isometry, conformal symmetry, the geodesic and deviation equations, and the conjugate point theorem, are all the same regardless of what type of field is being described. The geometric view provides a one stop shop for all classic ray theory, and ray trace implementation needs. One of the primary questions that this research seeks to address is how to generalize these concepts to ray paths in stochastic environments. A summary of this chapter is provided in Table 1.

Table 1 – List of all Eikonals, their origin(s), and references

Eikonal Versions				
Type	Approach	Equation	Geodesic	Sources
Classical	Helmholtz, Eq. (1)	$\left\|\vec{\nabla}\varphi\right\|^2 = n^2$	No	Kravtsov & Orlov [3]
	Covariant Wave Equation, Eq.(6)	$\left\|\partial_\mu \varphi\right\|^2 = 0$	Yes	Unruh [11], Visser [12]
	Maxwell's Equation, Eq. (7)			Schneider *et al* [9], Perlick [13]
	Method of Characteristics			Courant & Hilbert [1]
Exact	Helmholtz, Eq. (1)	Eq. (10)	No	Foreman [4, 14]
	Covariant Wave Equation, Eq.(6)	Eq. (13)	No	This text

3. NUMERICAL METHODS FOR THE EIKONAL EQUATION

As discussed in section 2, solving the Eikonal equation is a fundamental problem in wave mechanics. Although the Eikonal is often derived from a high frequency expansion of the Helmholtz equation its solutions, which encode the phase of the wave, actually provide insight at all frequencies. Thus, characterizing how solutions to the Eikonal vary in a noisy environment is a key issue for understanding wave propagation in random or fluctuating media in a variety of contexts. Due to its non-linear structure, it is difficult to treat the stochastic Eikonal equation analytically and numerical methods are needed. There are three broad classes of suitable methods:

- *Level-set methods.* These essentially simulate the propagation of a wavefront according to the Huygens-Fresnel principle. The wavefront is tracked by following level sets, *e.g.* where $\phi(x) = const$. Although intuitive to understand and straightforward to implement, these are not efficient and can suffer from numerical instabilities [21, 22].
- *Ray tracing.* The ray tracing approach arises from applying the method of characteristics to the Eikonal equation. As the name suggests, one imagines sourcing a ray at point q with "momentum" (direction) p and then (q, p) evolve according to a coupled set of 1st order differential equations that depend on the index of refraction $n(q)$ and its gradient. The actual Eikonal, *i.e* ϕ, is then determined by integrating the travel time along each ray. Individual ray trajectories can be solved efficiently and accurately but in stochastic, inhomogeneous environments it is necessary to do a "dense" ray-trace which is more demanding [23, 24].
- *Fast-marching methods.* The so-called fast-marching method is the preferred technique for finding global solutions to the Eikonal equation. This approach is motivated by the insight that $\phi(x)$ encodes *the shortest* travel time from the source (point or boundary) to x. Thus, the travel time to each point can be built up in a "greedy" fashion by first determining the shortest travel time to all nearby points that are closer to the source (like Dijkstra's shortest-path algorithm). Given this basic principle, different implementations use different approximations

for the travel time between volume elements and different heuristics for the order in which nodes are visited [21, 22].

More details on all three methods, include the specific implementation of each used for generating the data in this report, are provided below.

3.1 Level-set Method

Recalling ϕ as the phase of the wave-field, the time evolution of ϕ is given by: $\partial_t \phi(\vec{x}, t) + n(\vec{x})|\nabla\phi(\vec{x})| = 0$. Adopting a spatial discretization labeled by $\vec{x}_i$, this equation can clearly be approximately solved by the finite-difference rule:

$$\phi(\vec{x}_i, t + \Delta t) = \phi(\vec{x}_i, t) - \Delta t \cdot n(\vec{x}_i)|\nabla\phi(\vec{x}_i, t)| \tag{16}$$

where $\phi(\vec{x}_i, 0)$ is given as the initial data. To propagate a planar wavefront, for example, one may specify $\phi((0, y_i),0) = 0$ for $\phi((x_i > 0, y_i),0) = 1$. The difficulty in implementing this solution lies in accurately determining $|\nabla\phi(\vec{x}_i, t)|$. Estimating gradients in finite-element schemes is generically challenging, but here there is an additional subtlety: an "upwind difference" scheme must be used, or non-physical discontinuities in the phase will develop [21]. Essentially, care must be taken to propagate the wavefront away from the region through which it has already passed. Concretely, the simplest way to define an upwind difference is calculate the gradient at x_i only in "upwind" directions, *i.e.* towards points with a smaller phase. In 2D,

$$\begin{aligned} a|\nabla\phi(\vec{x}_i, t)| = (&\max(\phi(x_i, y_i) - \phi(x_{i-1}, y_i), 0)^2 + \min(\phi(x_{i+1}, y_i) - \phi(x_i, y_i), 0)^2 \\ &+ \max(\phi(x_i, y_i) - \phi(x_i, y_{i-1}), 0)^2 + \min(\phi(x_i, y_{i+1}) - \phi(x_i, y_i), 0)^2)^{\frac{1}{2}} \end{aligned} \tag{17}$$

where a is the length scale of the chosen discretization. Generalizations to 3D are straightforward, and more sophisticated upwind difference estimates may also be employed. A basic implementation of the level set method is quite computationally expensive, since the gradient must be evaluated at grid point every time step and $O(L)$ time steps must be taken to fully propagate the front, where L is the number of grid points along one direction of the system. This leads to a complexity of $O(L^{d+1})$, where d is the spatial dimension [21]. We will see below this compares unfavorably to the fast-marching method.

In numerical tests of simulating the propagation of plane waves through lenses, the level-set method was found to be significantly slower and less accurate than the fast-marching method. Therefore, it was not applied to the study of stochastic environments.

3.2 Ray Tracing

There are many excellent references on ray-tracing, see [23, 24]. Details only relevant to numerical studies on solving the Eikonal equation in a stochastic environment are reviewed here. For reasons that will be clear when the model for stochasticity is discussed, the following parametrization of the refractive index is chosen, $n(\vec{q}) = e^{\eta(\vec{q})}$ (note this is > 0 as long as η is real). In the arc-length parametrization of the ray equations, this leads to particularly nice expressions for the ray position $\vec{q}$ and direction $\vec{p}$. The variable $\vec{q}$ is chosen to specify points on the ray path, where as $\vec{x}$ labels arbitrary points in space.

$$\begin{aligned} \dot{\vec{q}} &= \vec{p} \\ \dot{\vec{p}} &= \vec{\nabla}\eta - \vec{p}\left(\vec{\nabla}\eta \cdot \vec{p}\right) \end{aligned} \tag{18}$$

The length of $\vec{p}$ is conserved in this formulation, which makes it convenient to choose a fixed dt for an Euler-like solution (it also provides a good additional check on convergence). In practice, it was found that (at least for the benchmarks and stochastic environments considered) the basic implicit midpoint method worked best for numerical integration.

3.3 Fast-marching Method

The fast-marching method (FMM) finds the viscosity solution to the static Eikonal equation $|\nabla\phi(\vec{x})|^2 = n^2(\vec{x})$ on a region Ω. It proceeds by propagating arrival times on the boundary $\phi(\vec{x}) = f(\vec{x}), \vec{x} \in \partial\Omega$ to the rest of the region in greedy manner. To implement the FMM it is helpful to maintain three data structures, *visited, front, unvisited*. The *visited* data is initialized to contain the boundary nodes and *unvisited* to contain all other nodes. The process iterates over the neighbors of *visited* and add them to *front,* sorted by value of ϕ propagated to the neighbor. The natural data structure to use for *front* is a priority queue, where high priority is given by a low value of ϕ at that node. The neighbors of *visited* added to *front* are also removed from *unvisited*. After this initialization, the main iterative step of the algorithm can proceed:

1. Pop the highest priority node, *N,* from *front*, add it to *visited.*
2. Iterate over the unvisited neighbors of *N*, removing them from *unvisited* and adding them to *front* according to the propagated value of ϕ
3. Repeat 1-2 until *unvisited* is empty

A key component of the algorithm is the numerical propagation of ϕ, which is done by solving for $\phi(\vec{x}_i)$ given its neighbors using the discretized static Eikonal equation. However, as in the level-set method, only upwind neighbors of $\vec{x}_i$ should plugged into the discretized equation – this guarantees that the shortest arrival time, also called the viscocity solution is found. To illustrate this, consider the 2D case explicitly. Assuming a Cartesian grid with lattice constant a, let $A = (x_i, y_i)$ be the point of interest and let $B = (x_j, y_i)$ be its upwind neighbor in the x-direction, $j = i \pm 1$ depending on whether the node to the left or right has a lower value of ϕ (an unvisited node should be treated as having infinite ϕ for this purpose). Similarly, let C be its upwind neighbor in the y-direction. Then the following equation must be solved:

$$\big(\phi(A) - \phi(B)\big)^2 + \big(\phi(A) - \phi(C)\big)^2 = n^2(A)a^2 \tag{19}$$

which is simply a quadratic equation for $\phi(A)$ and can be easily solved. Note, however, that a valid solution to the propagation must have $\phi(A) > \phi(B), \phi(C)$. For the solution to the above quadratic to have this property we must have $|\phi(B) - \phi(C)| < a \cdot n(A)$. If this condition is not satisfied, then the value $\phi(A)$ should be linearly propagated, $\phi(A) = \min\big(\phi(B), \phi(C)\big) + a \cdot n(A)$. Linear propagation corresponds to one the partial derivatives of ϕ vanishing at A. The generalization to 3D is straightforward, with the minor subtlety that one must account for the possibility that one or two partial derivatives of ϕ may vanish. For a more detailed introduction to the FMM see references [21, 22].

Using an efficient implementation of a priority queue, the runtime of the FMM is only $O(L^d \log L)$, saving (essentially) a factor of $L/\log(L)$ compared the iterative level-set method [21, 22]. In typical applications, this factor of $L/\log(L)$ is enormous since one wants to a take very fine discretization to ensure numerical accuracy.

The FMM described here can be improved in several ways. Most obviously, more sophisticated functions to estimate $|\nabla\phi(A)|$ by using longer-distance finite-difference stencils may be used, see [25] for details. It is also possible use precomputed / analytical solutions to Eikonal for linear or quadratic expansion of $n(A)$, so that small scale variation in n can be more easily accommodated [26]. However, these

improvements are primarily geared towards maximizing the acceptable coarseness of the discretization. For the study of simple models of stochastic environments such improvements were not necessary. Finally, it is worth noting that a marching method has been developed for both Eikonal *and* its 1-jet (gradient), so that the rays and Eikonal can be simultaneously determined [27].

3.4 Benchmarking FMM and Ray-tracing

The fast-marching method and ray-tracing are both useful approaches to numerically solving the Eikonal equation. It is important to understand how they compare and to benchmark both methods in exactly solvable refractive environments. In this section, we evaluate two such cases: a linear-wave speed profile and the Kormilitsin profile.

Linear wave speed:
Results

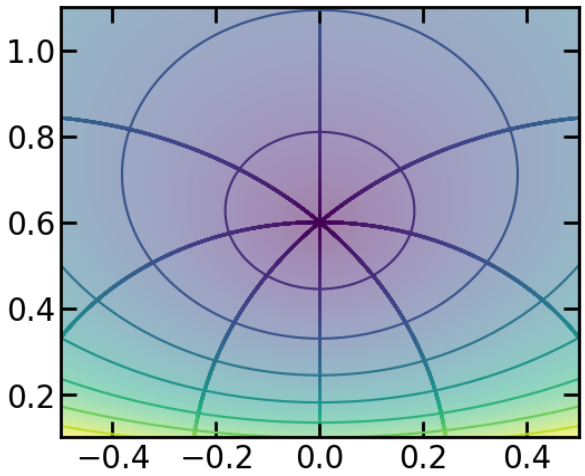

Figure 2 - Φ as determined by the FMM (indicated by color) and its contours for a linear wave-speed profile. The ray solutions (solid lines) are always perpendicular to the contours.

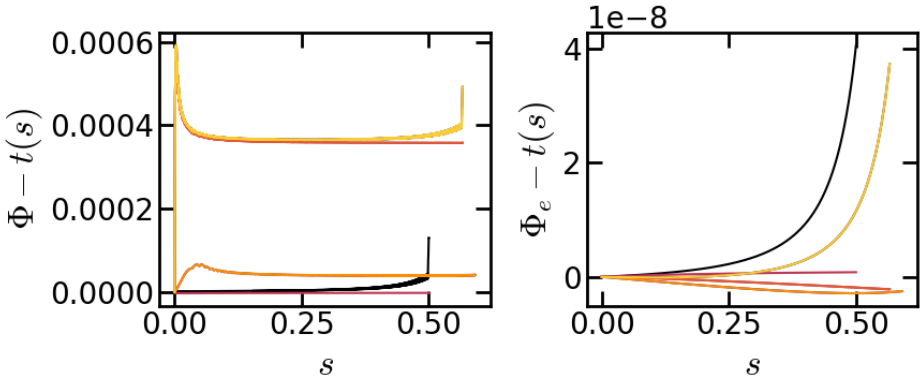

Figure 3 - Left: The error between Φ and the exact solution. The error is comparable to the discretization scale of 10^{-3}. Right: the error between Ray travel time and the exact solution. The error is significantly smaller, $O((dt = 2 \cdot 10^{-4})^2)$, since the implicit midpoint method used for integration is 2nd order errors.

Kormilitsin:
Results

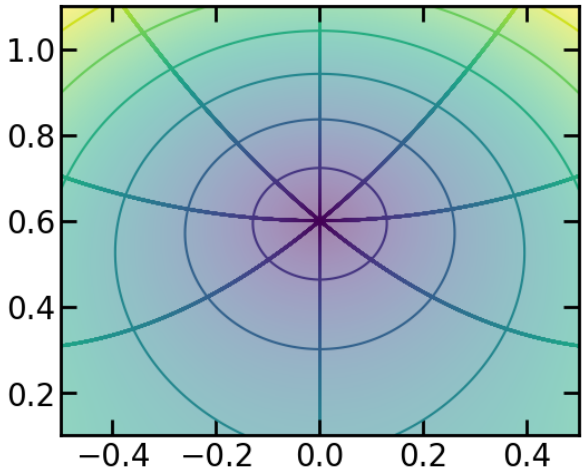

Figure 4 - Φ as determined by the FMM (indicated by color) and its contours for the Kormilitsin profile. The ray solutions (solid lines) are always perpendicular to the contours.

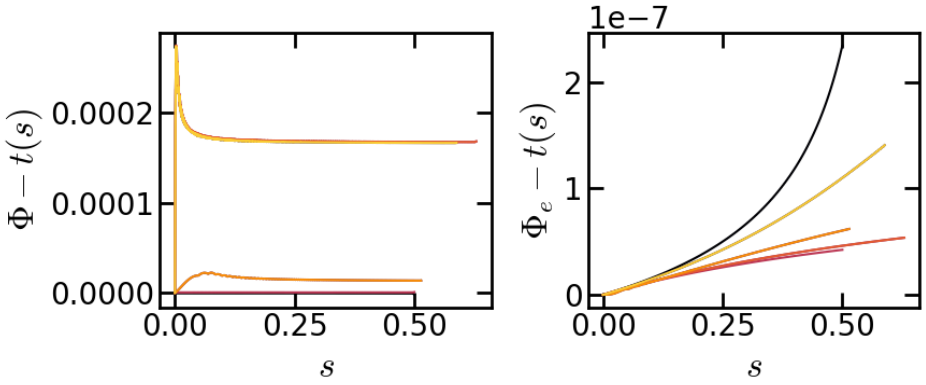

Figure 5 - Left: The error between Φ and the exact solution. The error is comparable to the discretization scale of 10^{-3}. Right: the error between Ray travel time and the exact solution. The error is again $O((dt = 2 \cdot 10^{-4})^2)$.

4. MODELING STOCHASTICITY

The benchmark cases of the previous section illustrate that the Eikonal solver and ray trace are providing consistent information for a smooth refractive profile. The technique is now extended to include randomness to a background profile for the purpose of evaluating stochastic behavior of the field. A general introduction to stochastic methods can be found in [28, 29]. In this section a Monte Carlo approach is applied, where some portion of the refractive index is selected at random but is an otherwise smooth differentiable function of position. There are many (indeed, infinite) noise models one may consider as driving the stochastic Eikonal. For simplicity, a translation invariant Gaussian process is chosen, specifically with a squared exponential kernel. This is a standard model in physics, signal processing and

machine learning, so only its most important properties are briefly reviewed here. A Gaussian process is defined through the expectation values for the first and second correlation functions. We will always use a zero-mean process,

$$\begin{aligned} \langle \eta(\vec{x}) \rangle &= 0 \\ \langle \eta(\vec{x})\eta(\vec{x}') \rangle &= \sigma^2 \exp\left[-\frac{(\vec{x}-\vec{x}')^2}{\xi^2} \right] \end{aligned} \tag{20}$$

where σ determines the overall scale of the noise and ξ sets the degree of spatial correlation. All the derivatives of $\langle \eta(x)\eta(x') \rangle$ are defined, so any particular sample from this Gaussian process will in fact be a smooth function. In particular, the partial derivatives η_{x_i} are themselves Gaussian processes with correlations functions

$$\begin{aligned} \langle \eta_{x_i}(\vec{x})\eta(\vec{x}') \rangle &= \frac{\partial}{\partial x_i} \sigma^2 \exp\left[-\frac{(\vec{x}-\vec{x}')^2}{\xi^2} \right] \\ \left\langle \eta_{x_i}(\vec{x})\eta_{x_j}(\vec{x}') \right\rangle &= \frac{\partial^2}{\partial x_i \partial x_j} \sigma^2 \exp\left[-\frac{(\vec{x}-\vec{x}')^2}{\xi^2} \right] \end{aligned} \tag{21}$$

Most importantly, η and $\nabla\eta$ are well-defined, so ray-tracing can be used without any complications in such a stochastic environment.

The above equations, however, do not make it clearly how to actually sample η and $\nabla\eta$. There are several possible approaches. A standard approach would be to choose a spatial discretization so that $\eta(\vec{x}) \to \vec{\eta} \equiv [\eta(\vec{x}_1), \eta(\vec{x}_2), \cdots]^T$. Then sampling $\vec{\eta}$ reduces to sampling correlated Gaussian noise, for which there are many standard methods, *e.g.* Cholesky decomposition of the correlation matrix. Naively, this involves finding a matrix square-root of an $L^D \times L^D$ correlation matrix (every point has some correlation with every other point), which is computationally expensive. It is possible to approximate the square root, but for a translation invariant Gaussian process this is unnecessary. A more efficient method for sampling is to use the Fourier transform. The correlation function between Fourier modes can derived straightforwardly and results in the simple form

$$\langle \eta(\vec{p})\eta(\vec{p}') \rangle = \delta(\vec{p}-\vec{p}')\, \sigma^2 \exp\left[\frac{-p^2\xi^2}{8} \right] \tag{22}$$

Conceptually, a translation invariant Gaussian process is nothing but a prescription for randomly sampling amplitudes of Fourier modes, given by the above formula. With this in mind, an efficient scheme for sampling from such a random process is clear. For concreteness, we will explain the scheme for the $\left[-\frac{1}{2},\frac{1}{2}\right] \times [-\frac{1}{2},\frac{1}{2}]$ unit square in 2D, but the method generalizes easily to higher dimensions. We first choose a uniform $L \times L$ discretization and periodic boundary conditions, which fixes $p_x, p_y \in \{0, 2\pi, 4\pi, \cdots L \cdot 2\pi\}$. We then sample an $L \times L$ matrix Q of i.i.d random complex numbers, according to

$$\left\langle Re\left[Q_{n_x,n_y}\right]^2 \right\rangle = \left\langle Im\left[Q_{n_x,n_y}\right]^2 \right\rangle = \sigma^2 \exp\left(-\frac{\left(n_x+n_y\right)^2 \pi^2 \xi^2}{2} \right) \tag{23}$$

with the real and imaginary component uncorrelated. Then, simply Fourier transforming Q and keeping the real part provides a sample of the process η on the $L \times L$ grid. This approach only requires building a matrix with L^D elements and can benefit from extremely fast implementations of the Fourier transform, such as those provided by the Julia package FFTW.jl.

Technically, due to the discreteness of the Fourier basis, this way of sampling only works well for correlation lengths that are not too large, *i.e.* $\xi \lesssim 0.1$ is required. However, this limitation can easily be overcome simply by scaling up the sampled noise in real space by a factor of b which take $\xi \to b\xi$. This requires interpolating between the grid points to evaluate η at points that were not originally defined in the grid. Although an approximation, this works extremely well in practice because, by definition, the function that is being interpolated is extremely smooth. A sample from a Gaussian process with $\xi = 1.0$ can be faithfully obtained by first sampling from a process with $\xi = 0.03$ on a grid with $L = 1024$ and then blowing up the resulting distribution by a factor of ≈ 33 (even using $L = 128$ does not actually result in significant interpolation artifacts). Example results of sampling followed by rescaling are included in the figures below.

A nice feature of the above method is that is easy to sample η and $\nabla\eta$ simultaneously. Indeed, after sampling Q, one can define $Q^x_{n_x,n_y} = i2\pi n_x Q_{n_x,n_y}$ and $Q^y_{n_x,n_y} = i2\pi n_y Q_{n_x,n_y}$. Then $\frac{\partial}{\partial x}\eta$ and $\frac{\partial}{\partial y}\eta$ are simply the real parts of the Fourier transforms of $Q^x_{n_x,n_y}, Q^y_{n_x,n_y}$ respectively. Examples of $\eta, \frac{\partial}{\partial x}\eta$, and $\frac{\partial}{\partial y}\eta$ are included in the figures below.

As mentioned above, this method of sampling generalizes straightforwardly the 3D. For details, see the implementation provided in [code ref].

Figures:

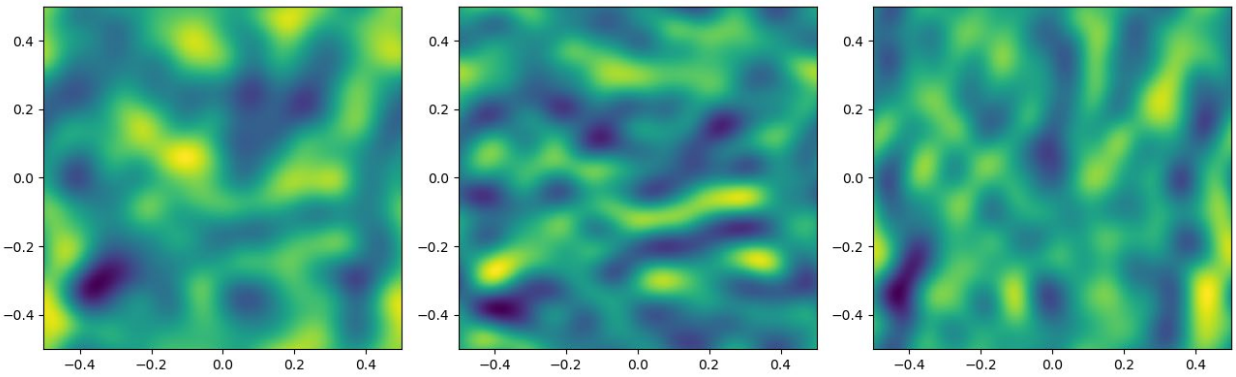

Figure 6 - Left: a sample of squared-exponential Gaussian process with $\xi = 0.1$; Middle: ∂_y derivative of the sample; Right: ∂_x derivative

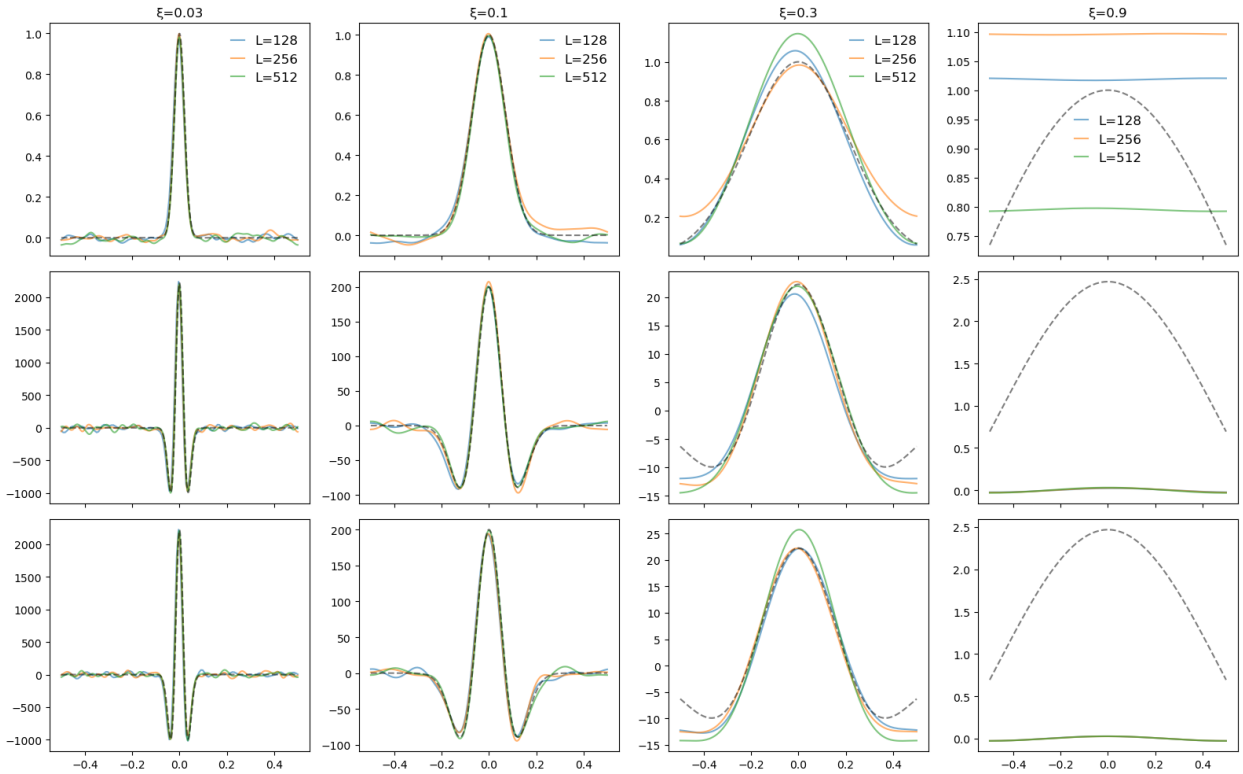

Figure 7 - Agreement between averaged sample correlation functions and exact correlation functions. For $\xi > 0.1$, there is systematic disagreement due to the finite number of Fourier modes used for sampling. For smaller correlation lengths, agreement is excellent. Top row: $\langle \eta(x)\eta(x') \rangle$ agreement; Middle row: $\langle \partial_x \eta(x) \partial_x \eta(x') \rangle$ agreement; Bottom row: $\langle \partial_y \eta(x) \partial_y \eta(x') \rangle$ agreement

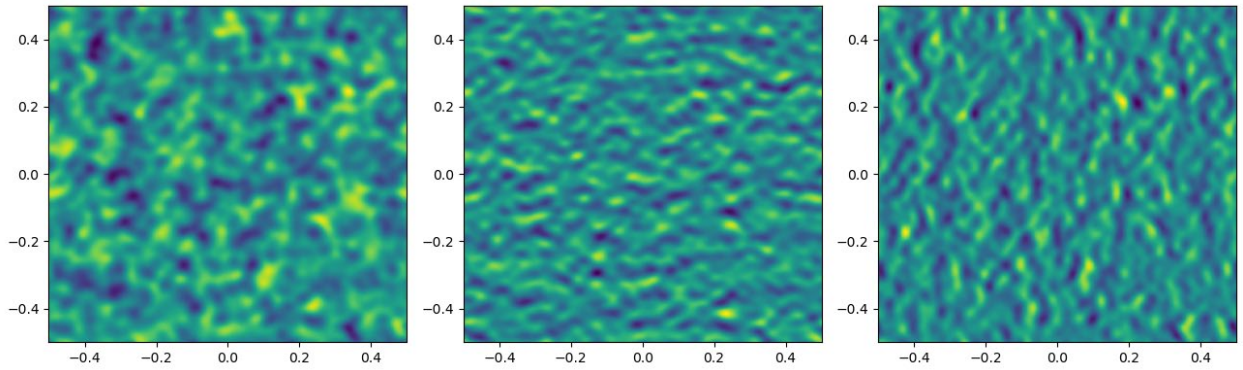

Figure 8 - Left: a sample of squared-exponential Gaussian process with $\xi = 0.03$; Middle: ∂_y derivative of the sample; Right: ∂_x derivative

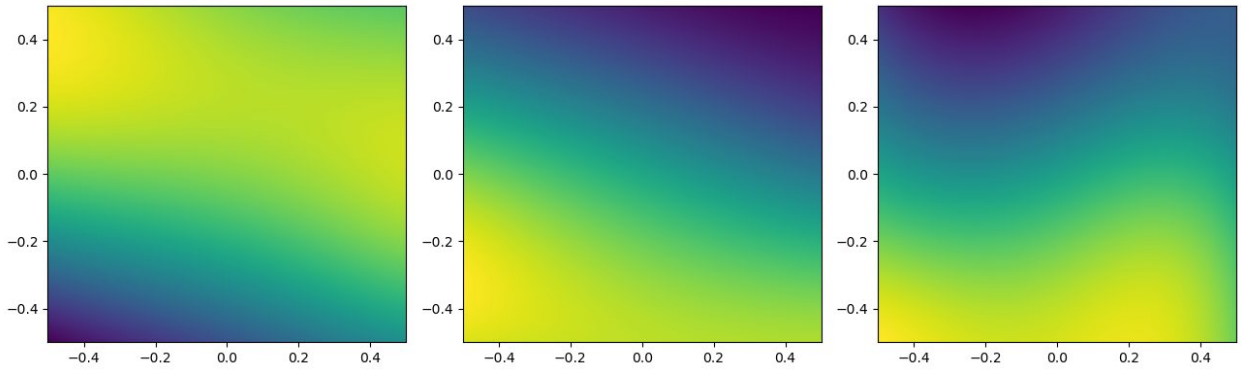

Figure 9 - Left: a sample of squared-exponential Gaussian process with $\xi \approx 1.0$ obtained from the above by 33.3x scaling; no artifacts from the scaling appear since the Gaussian process is (by definition) very smooth at the small scale which is interpolated. Middle: ∂_y derivative of the sample; Right: ∂_x derivative

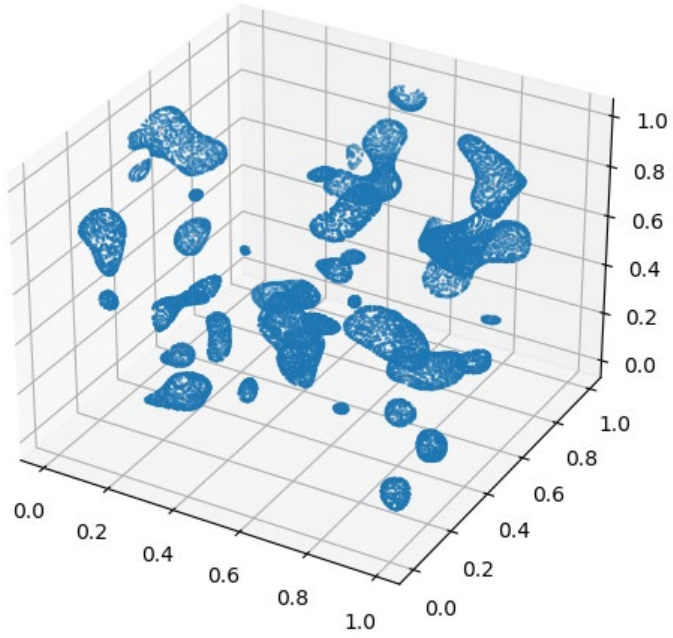

Figure 10 - Surfaces of constant magnitude in 3D Gaussian process sample with $\xi = 0.1$.

5. RAY TRACING AND FAST MARCHING IN A STOCHASTIC ENVIRONMENT

Ray-tracing and the fast-marching method (FMM) are both applied to the above model of a stochastic environment. Monte Carlo simulations are performed to characterize the basic statistics of the solutions, *e.g.* average travel time from the source, $\langle\phi\rangle$, and deviations from average travel time, $\langle\log\frac{\phi}{\langle\phi\rangle}\rangle$. (The expectation of the log of the ratio is preferred to *e.g.* the variance because the travel time is distributed over several orders of magnitude.) In 5.1, 5.2, a point source at the origin is considered as the boundary condition, and in 5.3, a plane wave emanating from the left side of the unit square is considered.

5.1 Rays as Random-walks

Before analyzing the statistics per se with the FMM, it is helpful to build some physical intuition by developing a conceptual picture of how the rays propagate in a stochastic environment. The simplest possible model is that the rays evolve as random walks driven by some noise with a correlation time, τ_c. In evaluating the utility of this picture there are two important questions: 1) to what extent does the direction of ray propagation actually de-correlate over its path and 2) what determines τ_c? Fortunately both these questions can be answered by looking at the correlation function $\langle p(\tau)p(0)\rangle$, where p is the instantaneous direction of the ray. The random walk picture should apply if $\langle p(\tau)p(0)\rangle$ decays to 0 roughly exponentially, and rate of decay is τ_c. On dimensional grounds the following is expected $\tau_c \propto \xi$, where ξ is the correlation length of the Guassian noise, but it will be seen that the dependence on σ is subtler.

First, consider the plausibility of the random-walk picture by examining some particular solutions.

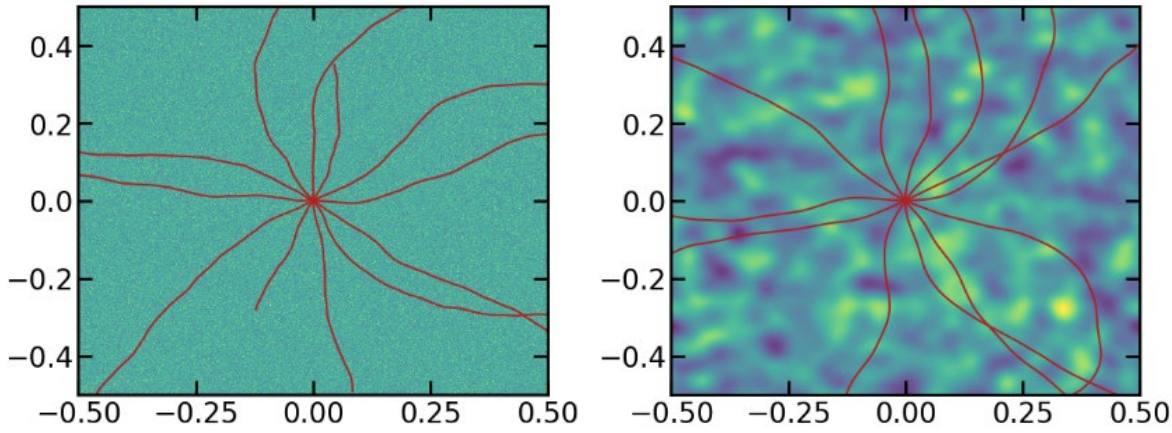

Figure 11Left: example rays with $\xi = 0.0004$ and $\sigma = 0.01$, Right: example rays with $\xi = 0.04$ and $\sigma = 0.1$

Although the rays retain some memory of their initial direction at the scale of the unit square, they are clearly deviating from their straight-line path with no discernable pattern. To be more rigorous, consider the momentum correlation function, for various noise correlation lengths ξ and noise amplitudes $\sigma = 0.01 \cdots 10$, indicated by green-purple shading. The correlation functions are evaluated over arc-length s.

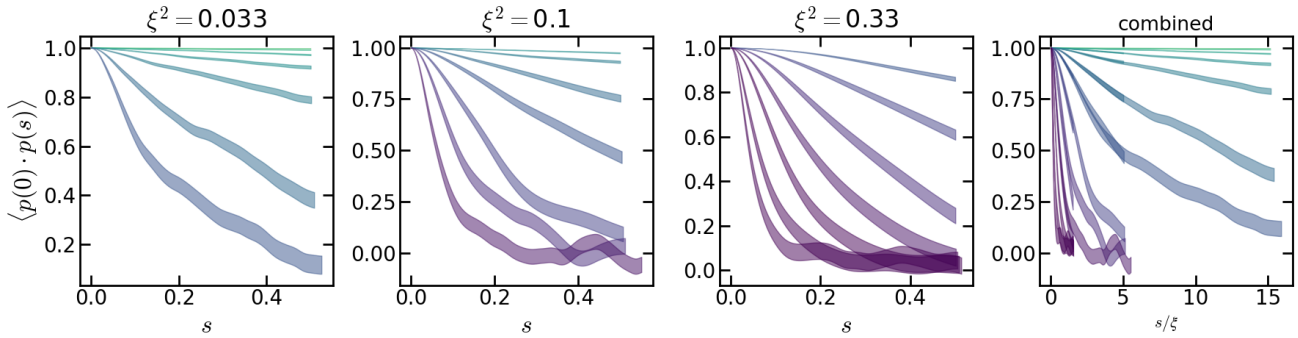

Figure 12 – Momentum correlation vs. arc-length for three values of ξ^2 (starting from the far left) and all combined (far right)

Clearly the momentum autocorrelation function tending to 0 in an exponential fashion in all cases, although exponential decay is sometimes quite mild for small noise-amplitudes. A one standard-deviation uncertainty in the correlation function is indicated by the shaded region.

It thus appears that the random walk model for the rays is at least a good "first-order" approximation, which leaves us with the question what determines τ_c. The value of τ_c can be extracted from the maximum slope of the decay. This slope is rescaled by ξ to make it unitless and comparable across noise realizations with different correlations lengths. The results are shown below.

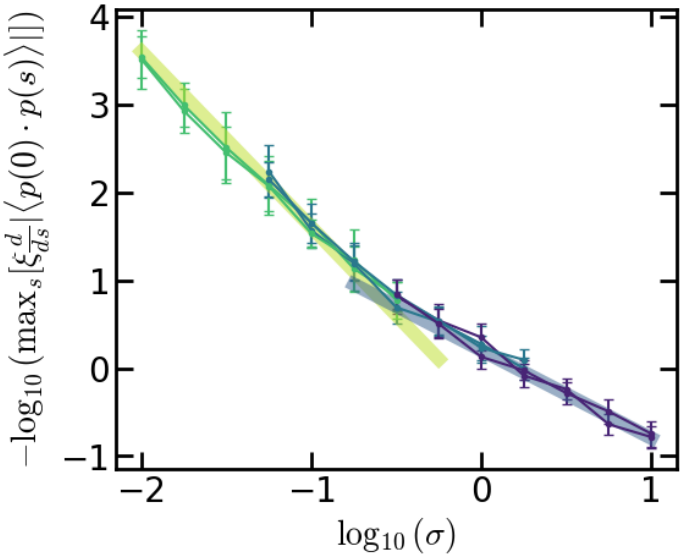

Figure 13 – Estimating τ_c from the maximum slope of the decay in Figure 11

Two distinct regimes are observed: $\tau_c \propto \frac{\xi}{\sigma^2}$ for $\sigma \ll 1.0$ (yellow shaded fit) and $\tau_c \propto \frac{\xi}{\sigma}$ for $\sigma > 1.0$ (blue shaded fit). Naively, it is somewhat surprising there are two scaling regimes for how τ_c depends on σ. To see why this occurs it is helpful to think about the limit of extremely strong noise, $\sigma \gg 1.0$. In this case, each ray will rapidly re-orient so that $p \parallel \nabla\eta$ (then $\dot{p} = 0$). Since $\nabla\eta$ is just a random direction, the time it takes for the re-orientation to occur is in fact the correlation time. The trajectory for rays for planar η is exactly solvable and it can be seen that this takes a time $\propto \frac{1}{\langle|\eta|\rangle} = \frac{1}{\sigma}$, which explains the scaling in the

large σ regime. On the other hand, a standard Markovian approximation for computing the correlation function yields the $\frac{1}{\sigma^2}$ scaling seen in the small σ regime.

The significance of this simple conceptual model is that it helps form rough estimates of the significance of noise in practical physical environments. For example, in atmosphere the noise on the index of refraction is quite small, typically $\delta n \sim 10^{-5}$ [25, 30]. The correlation length of this noise may range from mm to km, , but assuming a typical value of cm we obtain a correlation length of 10^8 m. This means that a beam sent over 10 km = 10^4 m will have an angular wander of around 10^{-4}, resulting in a displacement error of ~ 1 m. Note that this is a similar result to that obtained in [25] for wander due to turbulence using a much more complicated method that analyzed the ray equations perturbatively in noise.

5.2 Average travel-time from FMM

It is interesting to compare the picture of randomly propagating rays to the rather mild effects of stochasticity observed in the statistics of the FMM solutions. Consider an identical setup, with a point-source at the origin of the unit square, and determine the FMM travel time, ϕ, for an ensemble of noise realizations. The results are summarized below.

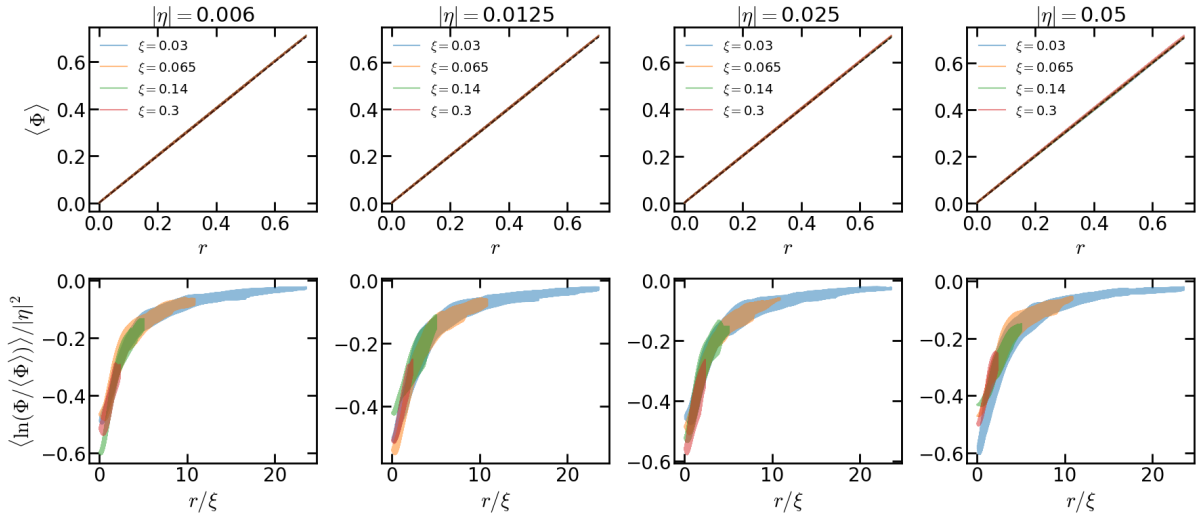

Figure 14 – Statistics of the FMM travel time solution in a stochastic medium

In the above figure $|\eta| = \sigma$, and r is the distance from the source (origin). The first thing to notice is that the stochastic environment has a negligible effect on the mean travel time (top row) – essentially $\langle \phi \rangle \approx r$ for all noise strengths and correlation lengths, which is the noise-free solution. This result can be derived by solving for moments of ϕ perturbatively in the noise strength, which shows that the first correction to the mean travel time appears at $O(|\eta|^2)$, which is quite small for all of the above. Investigating if this linear travel time result holds for $|\eta| \sim 1$ is an interesting direction for future research.

The fluctuations about $\langle \phi \rangle$ are more interesting. As mentioned above, the most natural way to quantify the fluctuations $\langle \log \frac{\phi}{\langle \phi \rangle} \rangle$ (bottom row) since near the origin fluctuations in travel time are very small and away from the origin they can be large. An interesting pattern emerges in these fluctuations – they collapse when rescaled by ξ and $|\eta|^2$, and are only significant near the origin while for $r > 10\,\xi$ they are negligible. Roughly speaking, it appears that near the origin there is always a "shortcut" through the

noise field to arrive at some nearby point more quickly, but over longer distances these shortcuts are cancelled out by obstructions. Of course the fact the fluctuations collapse when rescaled is not surprising given the preceding discussion of the scaling behavior of rays, but understanding the universal form to which they collapse is an interesting direction for future research.

5.3 Ray tracing vs. FMM

The above discussions surface a discrepancy between the ray-tracing and FMM solutions of the random Eikonal. At large distances, the rays have undertaken significant random walks meaning the travel time should be *longer* than in the noiseless case. On the other hand, the FMM solution show that at large scales the travel time is just proportional to distance; not at all what would be expected from a random walk. The resolution is that the rays *cross* and the FMM solution is the *minimum* travel time to a given point. Thus while many wandering rays may pass through a point distant from the origin, only one of them agrees with the FMM solution and matches the minimum travel time.

This is an important observation that warrants a deeper analysis. Indeed, it is quite important to know when the ray tracing solution and FMM solution unambiguously agree, since the FMM solution is typically faster and easier to compute. Conceptually, this is equivalent to the question of when multipathing makes an important contribution to the propagation. This is challenging question and the answer is not yet fully understood. Roughly speaking, it appears there is characteristic region around the source for which ray tracing and the FMM solution unambiguously agree. The size of this region is surely proportional to ξ, but its exact boundaries are hard to derive. An example of the expected behavior is shown below, where the ray solution (obtained by doing a dense ray trace) and the FMM solution are compared for a plane wave source on the left edge of the unit square. The noise parameters are $\xi = 0.02$ and $\sigma = 0.003$.

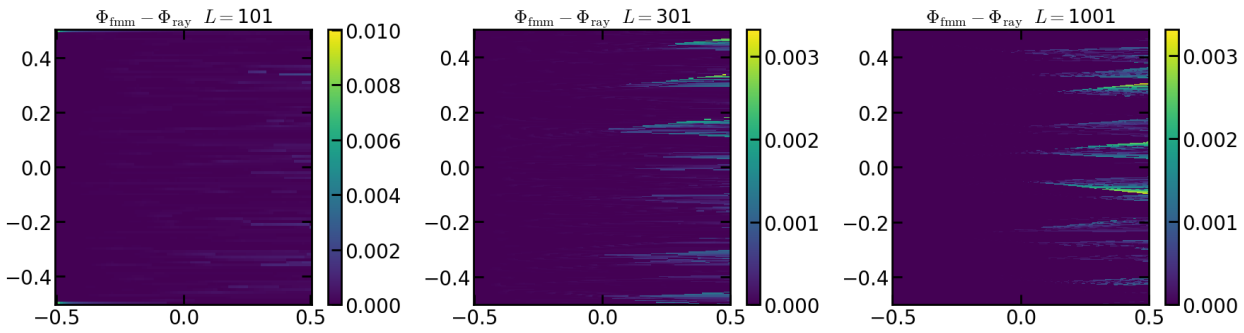

Figure 15 – Discrepancy between FMM and ray trace in a stochastic medium

A discrepancy between the ray solution and FMM solution arises at $x \approx 0$, independent of the discretization. To the right of $x \approx 0$, "showers" of deviation appear, which clearly evidence several rays crossing and then spreading back out. Understanding why the deviation appears at a distance of 0.5 from the source, and developing general understanding of the deviation between the ray solution and FMM, remains an important goal for future research.

6. DISCUSSION, CONCLUSION, SUMMARY

The main goal of this report is to present results of developing and benchmarking a numerical method for directly solving the Eikonal equation. This will serve as a tool in future studies for probing the statistics of physical and geometric properties of ray paths describing radio frequency propagation in random environments and for comparing results to other numerical stochastic solvers. Two of the main features of

interest are the time of first arrival from source to receiver, more generally travel time along a ray path, and caustic formation as well as other geometric properties of ray paths. The rational for developing the approach presented here is that the Eikonal method may be more efficient for evaluating arrival times in some cases. Similar studies using Monte Carlo methods appear in the literature applied to acoustic problems in seismology [32, 33]. Authors note that ray trace techniques estimate first arrival times that are slightly larger (indicating slower travel time) as compared to Eikonal methods in shadow zones behind an object. Otherwise, the two approaches match. This observation is explained by noting that Eikonal solvers naturally incorporate "diffractive wavefront healing" as they propagate. To elaborate, classical ray tracing may not produce results in shadow zones in a refractive media. The specific studies cited in [32] look at ray paths propagation in a medium with a small region filled with a different refractive index, including a hard boundary between the two regions. The mismatch between the ray trace and Eikonal travel times is attributed to the fact that diffraction is not naturally included in ray traces, whereas the Eikonal solver contains information about diffraction at each step that is incorporated in the logic for determining minimum time of arrival. Hence then term "wavefront healing". One criticism of these studies is that they do not include well known formulas and method for rays that interact with finite convex boundaries to create "diffraction rays" [34]. Similar results are demonstrated for ray propagation in a 2D environment with random pockets of refractive gradients [32, 33]. The benchmarking done in this report does not contain such exotic environmental or numerical features. If one makes the effort to take into account diffraction rays in a complete ray trace the results should match the Eikonal [34]. Regardless, the work demonstrated here illustrates that for ideal and weakly random environments where caustic formation is less likely, the two approaches provide reliable and comparable results. Finally, the type of media studied in seismology is modeled as a fractal function, making ray trace approaches difficult if not impossible due to the lack of differentiability of the wave speed profile [33]. Solving the Eikonal directly avoids the debate over how to define the stochastic derivative, casting the entire problem as one of direct integration. The fact that Eikonal solvers naturally select the leading portion of the wavefront (shortest travel time) makes them a better candidate for evaluating travel time statistics in a random environment. The ray trace method would be more appropriate (if not necessary) for the study of geometric quantities in the presence of stochastic noise.

The results presented in this report will be used to explore several more interesting questions:

- Region of agreement between FMM and ray tracing?
- When do rays cross on average creating interference?
- When are conjugate points encountered on average?
- How do FMM and ray tracing to compare to full EM solution in stochastic environment?
- More realistic models of randomness, *e.g*. combining stochasticity with atmospheric models.
- What is the statistics of travel time along as predicted by FMM and ray tracing?

AKNOWLEDGEMENTS

This work was supported by the Office of Naval Research through a 6.1 base program.

REFERENCES

1. R. Courant & D. Hilbert, *Methods of Mathematical Physics Volumes I and II* (John Wiley and Sons, New York, 1984).

2. D. Bergman, *Method of Characteristics Applied to Stochastic Maxwell's Equations in the Homogeneous Chaos Basis Expansion*, NRL/5310/MR—2023/5, Distribution Statement A: Approved for public release; distribution is unlimited. (2023).

3. Yu A. Kravtsov and Yu I. Orlov, *Caustics, Catastrophes, and Wave Fields Second Edition*, (Springer Series on Wave Phenomenon Volume 15, Springer, Berlin, 1999).

4. T.L. Foreman, *A Frequency Dependent Ray Theory*, ARL-TR-88-17, Approved for public release – Distribution Unlimited, 1988.

5. D. Ludwig, "Uniform Asymptotic Expansions at a Caustic", Comm. Pure and Applied Math., Vol. XIX, 215 – 250 (1966)

6. M. Porter and H. Bucker, "Gaussian beam tracing for computing ocean acoustic fields", Journal of the Acoustical Society of America 82, 1349-1359 (1987).

7. C. W. Misner, K. S. Thorne, and J. A. Wheeler, *Gravitation*, (Princeton University Press, Princeton, 2017)

8. G. B. Arfkin, H. J. Weber, and F. E. Harris, *Mathematical Methods for Physicists: A Comprehensive Guide, 7th Edition*, (Academic Press, Cambridge, 2012)

9. P. Schneider, J. Ehlers, and E. E. Falco, *Gravitational Lenses*, (Astronomy and Astrophysics Library, Springer-Verlag, New York, 1992).

10. D.R. Bergman, *Application of Differential Geometry to Acoustics: Development of a Generalized Paraxial Ray-Trace Procedure from Geodesic Deviation*, NRL/MR/7140—05-8835, Approved for public release – Distribution Unlimited, 2005.

11. W. G. Unruh, "Experimental black hole evaporation?", Physical Review Letters, Vol. 46, 1351 – 1353, (1981).

12. M. Visser, "Acoustic black holes: Horizons, ergospheres, and Hawking radiation", Classical and Quantum Gravity, 15, 1767-1791 (1993).

13. V. Perlick, *Ray Optics, Fermat's Principle, and Applications to General Relativity* (Springer-Verlag, Berlin, 2000).

14. T.L. Foreman, "An exact ray theoretical formulation of the Helmholtz equation", Journal of the Acoustical Society of America, 86, 234-246 (1989).

15. J. M. Nichols, D. V. Nickel and F. Bucholtz, "Vector beam bending via a polarization gradient", Optics Express, Vol. 30, No. 21, Optics Express 38907 (2022)

16. J. M. Nichols, T. H. Emerson, L. Cattell, S. Park, A. Kanaev, F. Bucholtz, A. Watnik, T. Doster, and G. K. Rohde, "A transport-based model for turbulence-corrupted imagery", Applied Optics, Vol. 57, No. 16, 4524–4536 (2018).

17. D. R. Bergman, "Internal symmetry in acoustical ray theory", Wave Motion, Vol. 43, No. 6, 508-516 (2006)

18. D. R. Bergman, "Symmetry and Snell's law", Journal of the Acoustical Society of America, 118 (3), Pt. 1, 1278-1282 (2005)

19. B. O'Neill, *Elementary Differential Geometry*, (Academic Press, San Diego, 1966).

20. S. Kobayashi and K. Nomizu, *Foundations of Differential Geometry: Volumes I and II*, (John Wiley & Sons, New York, 1963).

21. Sethian, J. A. Level Set Methods and Fast Marching Methods: Evolving Interfaces in Computational Geometry, Fluid Mechanics, Computer Vision, and Materials Science. 2nd edition, Cambridge University Press, 1999.

22. Sethian, J. A. "Fast Marching Methods." SIAM Review, vol. 41, no. 2, 1999, pp. 199–235, https://doi.org/10.1137/S0036144598347059.

23. V. Červený, *Seismic Ray Theory*, (Cambridge University Press, Cambridge, 2001)

24. O. N. Stavroudis, *The Optics of Rays, Wavefronts, and Caustics*, (Academic Press, New York, 1972)

25. Mahalov, Alex, and Austin McDaniel. "Long-Range Propagation through Inhomogeneous Turbulent Atmosphere: Analysis beyond Phase Screens." Physica Scripta 94, no. 3 (March 1, 2019): 034003. https://doi.org/10.1088/1402-4896/aaf32c.

26. Potter, Samuel F., and Maria K. Cameron. "Ordered Line Integral Methods for Solving the Eikonal Equation." Journal of Scientific Computing, vol. 81, no. 3, Dec. 2019, pp. 2010–50, https://doi.org/10.1007/s10915-019-01077-z.

27. Potter, Samuel F., and Maria K. Cameron. "Jet Marching Methods for Solving the Eikonal Equation." SIAM Journal on Scientific Computing, vol. 43, no. 6, 2021, pp. A4121–46, https://doi.org/10.1137/20M1366526.

28. H. M. Taylor and S. Karlin, *An Introduction To Stochastic Modeling 3rd Edition*, (Academic Press, San Diego, 1988).

29. S. Karlin and H. M. Taylor, *A First Course in Stochastic Processes Second Edition*, (Academic Press, San Diego, 1975).

30. Stapleton, J. et. al. "Natural Environmental Models for Shipboard Radars." NSWCDD/TR-99/151: Dahlgren Division, Naval Surface Warfare Center. 2001.

31. I. Karatzas and S. E. Shreve, *Brownian Motion and Stochastic Calculus*, (Graduate Texts in Mathematics, Springer, New York, 1991).

32. O. Witte, M. Roth and G. Müller, "Ray tracing in random media", Geophys. J. Int., Vol. 124, 159-169 (1996)

33. S. B. Ojo and R. F. Mereu, "The effect of random velocity functions on the travel times an amplitudes of seismic waves", Geophys. J. R. astr. Soc., Vol. 84, 606-618 (1986)

34. J. B. Keller, "Geometric Theory of Diffraction", Journal of the Optical Society of America, Vol. 52, No. 2, 116-130 (1962)

A. ANALYSIS OF RAYS AS RANDOM WALKS

This appendix presents an analysis of random walk properties of ray paths under restricted conditions. Two derivations are provided, supporting the observations made in the analysis of the correlation time of rays in random environments, section 5. In the first, it is assumed that the scale of the noise η is small and a Markovian approximation is applied to determine how the correlation time of the ray direction scales with the noise magnitude, finding $\sim|\eta|^{-2}$. In the second, the complementary limit of extremely strong noise is considered. It is argued that this case is well approximated by the exactly solvable case of a ray propagating on an unknown, but a linearly varying, index of refraction background. This exactly solvable case yields a different scaling of the correlation time with noise strength, $\sim|\eta|^{-1}$. These two regimes are reflected in the numerical analysis above.

Small Noise: The Markovian Limit

Consider an index of refraction e^{η}, where η is a 2D Gaussian process,

$$\langle \eta(x)\eta(x')\rangle = |\eta| \exp\left(-\frac{(x-x')^2}{\xi^2}\right) \tag{A.1}$$

The ray equations presented in Eq. () are used for this analysis. In this parametrization, p is always a unit vector. Let $p(0) = [1\ 0]^T$, *i.e.* the ray initially points along the *x*-axis. The following expressions follow for $\nabla\eta$ and $p(t)$, $\nabla\eta = |\eta'|[\cos(\theta)\ \sin(\theta)]^T$, and $p(t) = \left[\cos\big(\delta(t)\big)\ \sin\big(\delta(t)\big)\right]^T$, $\delta(0) = 0$. An equation of motion for δ can be determined:

$$\frac{d}{dt}\sin(\delta) = |\eta'(q)|\big(\sin\big(\theta(q)\big) - \cos\big(\theta(q) - \delta(t)\big)\sin\big(\delta(t)\big)\big) \tag{A.2}$$

Where q implicitly depends on t. Using standard trigonometric identities,

$$\frac{d}{dt}\sin(\delta) = |\eta'(q)|\cos\big(\delta(t)\big)\sin\big(\theta(q) - \delta(t)\big) \tag{A.2}$$

And, after taking the derivative and cancelling terms the following simple form is obtained:

$$\dot{\delta} = |\eta'(q)|\sin\big(\theta(q) - \delta(t)\big) \tag{A.3}$$

Thus, the variance of δ grows according to:

$$\frac{d}{dt}\langle\delta^2\rangle = 2\langle\dot{\delta}\delta\rangle = 2\left\langle\int_0^t \big|\eta'\big(q(t)\big)\big|\sin\Big(\theta\big(q(t)\big) - \delta(t)\Big)\big|\eta'\big(q(s)\big)\big|\sin\Big(\theta\big(q(s)\big) - \delta(s)\Big)\,ds\right\rangle \tag{A.4}$$

Now we must begin making approximations to proceed. Since we are assuming small noise, $|\delta|$ increases slowly and we can linearize,

$$\frac{d}{dt}\langle\delta^2\rangle = 2\left\langle \int_0^t |\eta'(q(t))| \sin\left(\theta(q(t))\right) |\eta'(q(s))| \sin\left(\theta(q(s))\right) ds \right\rangle + O(\delta^2) .$$

Where terms linear in δ vanish due to the fact $\langle\cos(\theta)\sin(\theta)\rangle$ will average to 0 as θ varies from 0 to 2π. Now we again make use of the fact that we are assuming small noise, i.e. $|\eta'| \ll 1/\xi$, where ξ is the correlation length of the noise. This means that the integral will average to 0 for $|q(s) - q(t)| > \xi$. Since the ray is always moving with unit speed, and δ is changing slowly (again because the noise is small), this should be the case for all $s < t - \xi$. We can then make a very rough approximation that for all $s > t - \xi$, $q(t) = q(s)$ and $\theta(t) = \theta(s)$. This gives,

$$\frac{d}{dt}\langle\delta^2\rangle = 2\langle\xi|\eta'(q(t)|^2 \sin^2(\theta(t))\rangle \tag{A.5}$$

Taking the expectation value over the noise distribution (so θ is varies over 0 to 2π), and noting that $|\eta'| \sim |\eta|/\xi$, where $|\eta|$ is the noise scale, we have the simple result:

$$\frac{d}{dt}\langle\delta^2\rangle = \frac{\pi|\eta|^2}{\xi} \tag{A.6}$$

We can naturally define the correlation time of the ray as the time at which the variance exceeds some threshold value, so $\tau_c^{ray} \sim \xi|\eta|^{-2}$ as claimed.

Large Noise: Rapid Re-Orientation

We now consider the case when $|\eta'| \gg 1/\xi$, so the noise causes the ray path to rapidly align with the local gradient. Since the local gradient direction is uncorrelated with the initial ray direction, the time it takes for the alignment to happen is itself the correlation time of the ray direction. For large enough noise strength $|\eta|$, it is a good approximation to solve the ray equations assuming constant $\nabla\eta$. In this case, it is convenient to adopt coordinates such that $\nabla\eta = [|\eta'|\ 0]^T$ and the ray direction $\delta(0) = \theta$, where θ is the initial discrepancy between ray-direction and local gradient. Then, the ray equations reduce to

$$\dot{\delta} = -|\eta'|\sin(\delta) \tag{A.7}$$

which can be solved exactly,

$$\tan\left(\frac{\delta(t)}{2}\right) = e^{-|\eta'|\,t}\tan\left(\frac{\theta}{2}\right) \tag{A.8}$$

The key point is that after a time of order $1/|\eta'|$ the RHS will be small so that $\delta(t)$ must also be small, *i.e.* the ray will have aligned with the local gradient. Hence, we must have $\tau_c^{ray} \sim \xi|\eta|^{-1}$, as seen in the numerical results in the strong-noise regime.